Tribology International 194 (2024) 109531

Contents lists available at ScienceDirect

Tribology International

journal homepage: www.elsevier.com/locate/triboint

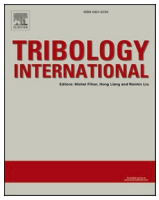

Assessment of benzoxazine resins as brake pad friction material binder: Tribological properties and PM emission

Davide Carlevaris *, Luca Fambri, Cinzia Menapace, Giovanni Straffelini

Department of Industrial Engineering, University of Trento, Trento, Italy

ARTICLE INFO

Keywords:
Brake pad friction material
Pin-on-Disc
Benzoxazine resin
PM emission

ABSTRACT

This study explores benzoxazine resins as alternative binders for brake pad friction materials, comparing them to the established phenolic resins. Benzoxazine resins feature great thermal properties, alongside industrially-attractive properties such as forgiving storage conditions and extended shelf life. Tribological Pin-on-Disc tests were conducted at different temperatures, with airborne emission monitoring. The characterization of the samples and their worn surfaces was carried out through TGA, SEM, and EDXS analyses. The results revealed promising tribological performance for benzoxazine-bound materials, suggesting potential environmental benefits, especially in high-temperature conditions. This research builds upon a preliminary study focusing on the processing aspects of benzoxazine resins.

1. Introduction

Disc brake systems are the most diffused brake system in the automotive field. The task of such system is to reliably slow down a vehicle in a secure manner. This is achieved through the dissipation of the kinetic energy into heat, which causes an increase of the temperature of the braking system itself. A disc braking system is composed by a calliper, ensuring the pressure application, a rotor, known as the disc, and a friction material lining, commonly referred to as brake pad. Typical automotive brake pads are composed of numerous ingredients, which can be broadly categorized into four groups: reinforcing materials, friction modifiers, fillers, and binders.

Although there are different types of binders, the most established ones in the automotive industry are resin binders. They constitute the matrix of the friction material composite and are therefore the components responsible for providing structural integrity to the material. In traditional automotive applications, such as light-duty vehicles and trucks, phenolic resins are the most commonly used binders [1] due to their cost-effectiveness and satisfactory thermal properties. Thermal properties are crucial for brake systems, as excessive friction material temperature during operation can lead to the degradation of the binder, thus causing increased wear [2,3] and, above a certain temperature threshold, a significant rise in the emission of sub-micrometric particulate matter (PM_1) [3–6]. Wear and PM emission by brake system have been shown to be an environmental hazard, affecting both the environment [7–10] and the human health [6,10–15]. Nevertheless, phenolic resins show some limitations, including the evolution of harmful gaseous species during curing, and a limited shelf life [16–18], primarily related to their susceptibility to moisture.

A relatively new class of resins called *polybenzoxazines* or *benzoxazine resins* offers appealing characteristics for binder applications. Although first synthesized in 1944 by Holly and Cope [19], they have only recently gained industrial interest thanks to the pioneering work of Ishida et al. [20–22]. Their excellent mechanical and thermal properties [23–26] make them strong contenders as binders for brake pads. Additionally, benzoxazine resins exhibit other advantageous qualities, such as dimensional stability, minimal byproduct formation during curing, low moisture absorption, and an almost-unlimited shelf life [21,27,28]. Unlike the condensation polymerization process of conventional phenolic resins, the crosslinking mechanism of benzoxazine resins consists of a ring-opening polymerization [29–31], which is a type of addition polymerization. This mechanism is a thermally activated process that does not require any additional crosslinking agent, and it allows for an extremely long shelf life, which is a really attractive property

Abbreviations: COF, Coefficient of friction; μ, Coefficient of friction.; Ka, Specific wear coefficient; PoD, Pin-on-Disc; RT, Room temperature; OPS, Optical Particle Sizer; SEM, Scanning Electron Microscope; EDXS, Energy Dispersive X-ray Spectroscopy; BSE, Backscattered Electrons; SE, Secondary Electrons; PM, Particulate Matter; TGA, Thermogravimetric Analysis; DTG, Differential Thermogravimetric Analysis; SS, Steady-state.

* Corresponding author.
E-mail address: davide.carlevaris@unitn.it (D. Carlevaris).

https://doi.org/10.1016/j.triboint.2024.109531
Received 11 January 2024; Received in revised form 28 February 2024; Accepted 8 March 2024
Available online 11 March 2024

from an industrial point of view, alongside minimal volumetric changes and volatile byproduct formation during curing. Benzoxazine resins also feature well-developed intra- and inter-molecular hydrogen bonding, providing unexpectedly good mechanical properties and resistance to moisture [21,24,31,32]. Furthermore, the chemical structure of benzoxazine resins is highly customizable [33–35], offering the potential to tailor their properties according to specific applications. Furthermore, the volatile byproducts of their curing and degradation process have been shown to be less toxic than those produced by phenolic resins, e.g. formaldehyde [23,36,37].

Some authors have explored the possibility of substituting phenolic resin with benzoxazine resin as brake pad friction material binder. Jubsilp et al. [38] compared a phenolic- and benzoxazine-bound laboratory-made friction material composition using a Pin-on-Disc tribometer, also investigating different percentage additions of UFNRP (ultra-fine full-vulcanized acrylonitrile-butadiene rubber particles). The materials bound by benzoxazine resins showed lower overall wear. Gurunath et al. [39] obtained promising results testing several types of benzoxazine resins in friction material compositions on a full-scale brake dynamometer. Lertwassana et al. [40] investigated the effects of aramid pulp and carbon fiber on friction materials using polybenzoxazines binder. However, current studies lack a comprehensive analysis of the material properties, either disregarding some important parameters strongly dependent on the binder such as wear, or the characterization of the friction materials. Most importantly, none of these studies has investigated the effect that the adoption of a different type of resin has on the PM emission of the friction material, which is becoming a crucial parameter for the future of brake pad materials [41,42]. Furthermore, no insight was provided regarding how the processing of the binder, in particular of the newly adopted benzoxazine resins, affects the properties of the friction material, although manufacturing parameters have been shown to be influencing the properties of the final product [43–47].

The present work is a continuation of the preliminary study [48] which focused on the characterization of the benzoxazine resin binders. Therefore, this work aims to assess the possible advantages related to the adoption of benzoxazine resin binders as substitutes of the conventional phenolic resins. Following our previous work, an optimization of the production process was hereby possible. Friction material compositions using benzoxazine and phenolic resin binders were compared by Pin-on-Disc testing at room and at high temperature. PM_{10} emission was also monitored. The contact surfaces of the tested materials were then characterized by SEM and EDXS analysis.

2. Materials and methods

2.1. Sample preparation

Two different benzoxazine resins, hereby codenamed “R6″ and “R7″, were supplied by Huntsman Ltd. These two resins are respectively based on BA-a and BF-a monomers, shown in Fig. 1, and are two of the most simple representative of the multifunctional benzoxazine family. As reference resin, a conventional *Novolac phenolic resin* binder was also used. A commercial low-metallic friction material mixture, devoid of any binder component, was used to produce the friction material samples. The elemental composition of the mixture, obtained by EDXS analysis, is shown in Table 1. Some of the included ingredients are also shown inside a friction material sample in Fig. 2. Grey cast iron discs, directly extracted from a C-segment car brake disc and having a hardness of 258 HV10, were used as rotating counterface.

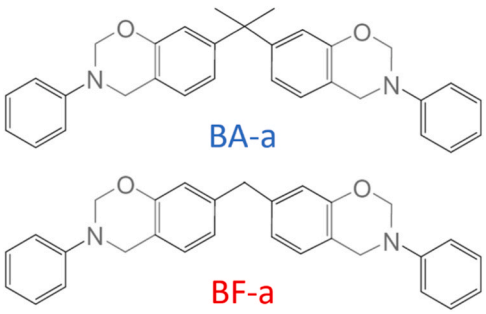

Fig. 1. Base monomers of the benzoxazine resins employed during this study: BA-a for R6 and BF-a for R7.

Three different friction material compositions were prepared by mixing the commercial friction material mixture (see Table 1) with 7 wt % of Ph, R6 and R7 resins in powder form. Each composition was mixed for 15 min using a *WAB T2F turbula mixer* to ensure proper mixture homogeneity. For each composition, three cylindrical pin samples having diameter and height of 10 mm were produced by hot moulding and curing. The hot moulding stage was performed by pouring the homogenized mixture in a special tool steel die, which was then inserted into a *Remet IPA30 mounting machine* and subjected to the desired processing parameter. Halfway through this step, the pressure was briefly released to allow for the evacuation of any gaseous byproduct inside the friction material. The curing stage of the self-sustaining cylindrical samples was then performed in a muffle furnace, in order to ensure complete curing of the binder. Different parameters were used during these two stages depending on the resin binder type, as schematized in Fig. 3.

The friction materials thereby produced were codenamed 7Ph, 7R6 and 7R7, respectively referring to the materials bound by Ph, R6 and R7 resin. Please note that the production process was designed based on the thermal analyses (DSC and TGA) carried out in the previous part of this work [48].

2.2. Testing and characterization

The tribological testing of the friction material samples was carried out using a *Ducom DHM-600* Pin-on-Disc (PoD) tribometer, schematized in Fig. 4. Grey cast iron discs with hardness of 258 HV10 were used as counterface. Before being used, each disc was thoroughly cleaned via a special degreaser and acetone, and sanded with a 180 grit SiC abrasive paper, to ensure no unwanted residue from the cutting process was present on the surface. Before testing, each sample underwent a run-in procedure, under the same contact pressure and sliding velocity conditions used for the test, for a duration of at least 30 min, in order to ensure that a complete conformal contact was reached between the surfaces of the pin and the counterface disc. The actual tests consisted in a continuous sliding of 90 min under an applied load $F_N = 79$ N (contact pressure $P_C = 1$ MPa), with a sliding velocity $v_S = 1.51$ m/s. These test parameters are representative of mild braking conditions, and were shown in a previous study to be able to satisfactory correlate with dynamometric bench results [49] when comparing two different friction material formulations. Each sample underwent PoD testing under these conditions both at room temperature and at a controlled high

Table 1
EDXS analysis of the commercial friction material composition.

Element	Mass (%)
O	11.6 ± 1.2
Na	0.9 ± 0.2
Mg	11.0 ± 1.5
Al	10.5 ± 0.9
Si	5.6 ± 0.5
S	6.5 ± 0.6
Ca	3.3 ± 1.0
Cr	3.5 ± 0.4
Mn	0.1 ± 0.1
Fe	28.1 ± 3.8
Zn	13.4 ± 1.5

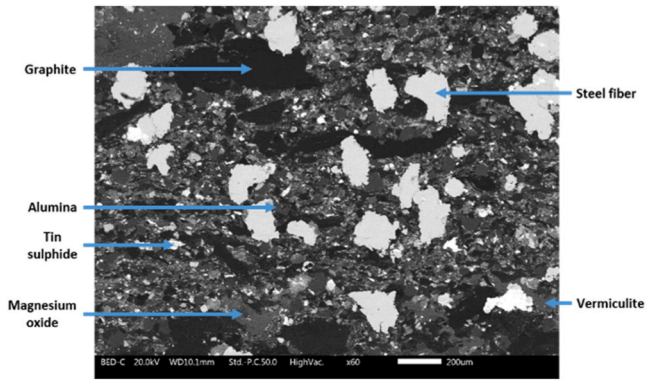

Fig. 2. SEM micrograph of the cross-section of a friction material sample showing some of the composition ingredients.

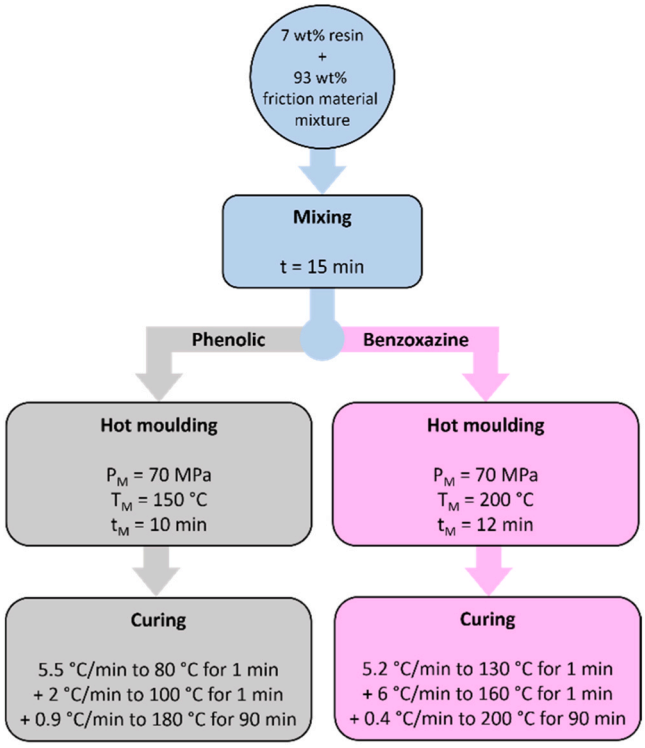

Fig. 3. Flowchart for the sample preparation of the friction materials pin samples.

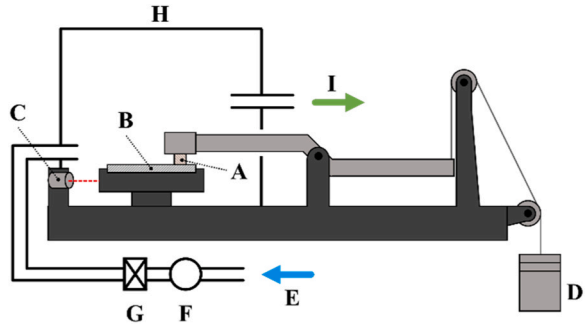

Fig. 4. Schematization of the PoD equipment. Pin (A), disc counterface (B), thermal sensor (C), applied load (D), ambient air (E), fan (F), HEPA filter (G), stainless steel chamber (H), air outlet to the OPS (I).

temperature of 430 °C. The temperature control was carried out by the PoD instrument itself by means of a resistance heating and water cooling system, coupled with a built-in thermal sensor, which managed the temperature of the disc holder. An analytical balance with a sensitivity of 10^{-4} g was used to measure the mass of the pins before and after every test. The friction coefficient μ was recorded in 1 s intervals by the tribometer, while the *specific wear coefficient* Ka, representative of the volumetric wear, was calculated following Eq. (1):

$$Ka = \frac{V_W}{F_N \bullet s} \quad (1)$$

Where V_W is the wear volume, F_N is the applied normal load, and s is the total sliding distance. The gravimetric wear was instead calculated by dividing the mass loss by the sliding distance.

In order to investigate the airborne PM_{10} emission, the PoD equipment was enclosed in a metallic chamber with a clean air inlet and an outlet connected to a *TSI OPS model 3330*. The clean airflow at the inlet was set at 14.1 l/min, while the OPS sampled air from the chamber at a self-controlled rate of 1 l/min. Consequently, the chamber was overpressurized, thus avoiding any contamination from the external ambient air. The OPS (Optical Particle Sizer) has a detection range of 0–3000 particles/cm^3, and measures the number of airborne particles having an airborne diameter in the 0.3–10 μm range dividing them in 16 channels (stages). Due to limitation of the PoD equipment, the airborne PM measurement could only be carried out for the room temperature tests.

7Ph and 7R7 samples underwent TGA (Thermogravimetric Analysis) under air atmosphere with a heating rate φ = 10 °C/min using a *Netzsch STA 409 Luxx* thermal analyser.

The characterization of the contact surfaces was carried out using a *JEOL JSM IT300LV* scanning electron microscope (SEM). The elemental composition was also investigated via EDXS analysis using the same equipment.

3. Results and discussion

3.1. Material characteristics

Table 2 shows the density and the mass loss experienced during curing by the produced samples. In this study, the benzoxazine-bound 7R6 and 7R7 showed higher density respect to that of 7Ph. Furthermore, the curing mass loss of 7R6 and 7R7 was also lower than that of 7Ph, suggesting that the production process was carried out properly, in contrast with the results obtained in our previous study [48], where the processing conditions for benzoxazine resins could not be satisfied. In fact, the benzoxazine-bound materials were expected to have higher density, thanks to the lower resin melt viscosity and lower gaseous byproduct production during curing [18,22] of benzoxazine resins, which was also partially confirmed by the lower mass loss during curing of neat R6 and R7 [48]. A lower melt viscosity helps the binder in filling the voids in the material during the production process. The higher gaseous byproduct formation of phenolic resins could cause the formation of voids and cracks in a composite material [18].

Fig. 5 shows the TGA and DTG (Differential Thermogravimetric Analysis) curves of 7Ph and 7R7. While the curve decline starts at a similar temperature for the two materials, the benzoxazine bound 7R7 shows a slower mass loss, indicating better resistance to thermal degradation respect to phenolic resin. This is further highlighted by the higher DTG curve once in the 300–500 °C range.

Table 2
Density and curing mass loss of the produced friction materials.

Friction material	Density (g/cm^3)	Curing mass loss (%)
7Ph	2.42 ± 0.04	0.43 ± 0.04
7R6	2.55 ± 0.02	0.15 ± 0.06
7R7	2.58 ± 0.04	0.11 ± 0.03

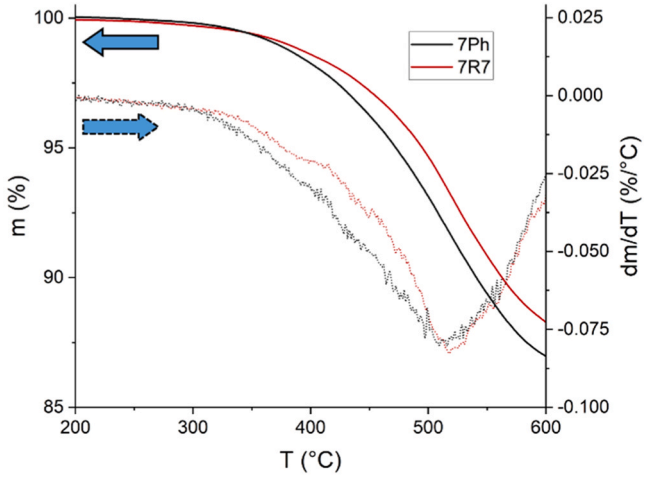

Fig. 5. TGA and DTG in air atmosphere of the 7Ph and 7R7 friction materials.

3.2. Room temperature results

Fig. 6 shows the average friction coefficient curves of the tested compositions. 7Ph, 7R6 and 7R7 all showed similar behaviour. All curves show the typical features of friction material dry sliding: initially a *run-in* phase takes place, involving a fast increase in the friction coefficient; then the μ value stabilizes, reaching the stage known as *steady-state* regime.

Table 3 shows the tribological and emission results obtained from the tests performed at room temperature. The friction coefficient at the steady-state μ_{SS} was comparable for all the materials, which was expected since resin was the only component changing between the different compositions. The gravimetric wear was also extremely similar for the tested materials, while 7Ph showed higher volumetric wear, represented by Ka. This seemingly unexpected result can be explained by the difference in density of the materials (see Table 2). In fact, the simple sum of the 6.0% density difference and the 1.9% gravimetric wear difference almost equals the 8.1% difference in volumetric wear observed between 7Ph and the benzoxazine-bound 7R6 and 7R7. Nevertheless, the difference in volumetric wear is a meaningful result, since the dimensions of a brake pad are fixed, and translates in a longer operational lifespan in case of 7R6 and 7R7. Ka/μ is a parameter which represents the amount of volumetric wear produced per unit of dissipated friction power. While the whole friction power is not used for its calculation, the

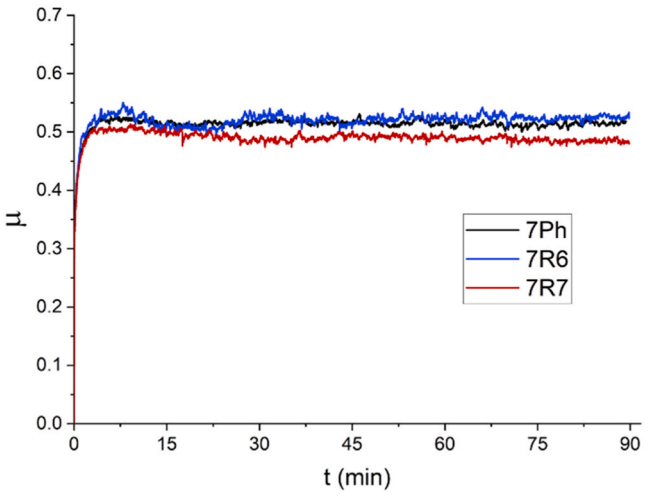

Fig. 6. Average PoD friction coefficient curves for the tested friction material compositions at room temperature.

Table 3
Tribological and emission results obtained from the PoD tests performed at room temperature.

Friction material	μ_{SS} (-)	Gravimetric wear (mg/km)	Ka (10^{-14} m^2/N)	Ka/μ (10^{-14} m^2/N)	$PM_{Conc\text{-}SS}$ (#/cm^3)
7Ph	0.51 ± 0.03	5.1 ± 0.4	2.67 ± 0.22	5.26 ± 0.29	569 ± 147
7R6	0.52 ± 0.01	5.0 ± 0.5	2.46 ± 0.25	4.77 ± 0.36	603 ± 122
7R7	0.49 ± 0.02	5.0 ± 0.3	2.45 ± 0.10	5.05 ± 0.24	556 ± 81

friction coefficient μ is sufficient since the dissipated power P_{diss} follows Eq. (2):

$$P_{diss} = \mu \bullet F_N \bullet v_S \quad (2)$$

Where F_N and v_S are fixed parameters, and thus P_{diss} is directly proportionate to μ. Note that in this case μ is the average COF registered across the whole test and not the one reached at the steady state μ_{SS}. Once again, Ka/μ shows how the volumetric wear per unit of dissipated power was higher in case of 7Ph. Respect to our previous work [48], the overall lower wear shown by the benzoxazine-bound materials further suggests that the improved processing of the binder could lead to an improvement in the tribological properties of the whole friction material composition.

Similarly to the previous friction coefficient and mass loss results, the PM_{10} airborne particle concentration at the steady state $PM_{Conc\text{-}SS}$ was comparable between all the tested materials. The differences in this regard are marginal and within margin of error between each other, thus also partially reflecting the differences observed regarding μ_{SS} and wear. Nevertheless, their overall behaviour appears coherent with that of the dissipated power, i.e. higher COF favours higher wear and emission.

Fig. 7 shows the number distribution and the mass distribution profiles of the friction materials airborne emission respect to the size of the airborne particles. Note that while the number distribution was directly measured by the OPS, the mass distribution is an approximation. In fact, for the calculation of the approximated mass distribution, the airborne particles were considered spherical and with constant density. All distributions are extremely similar, showing a three modal shape which is partially congruent with previous literature [50–52], thus indicating that the mechanisms for the formation of the airborne particulate matter were the same for all the materials. However, the positions of the distribution peaks are slightly different for the number and mass distributions: they are in the 0.374–0.465 μm, 0.897–1.117 μm and 1.391–1.732 μm OPS stages for the number distribution while they are found in the stages immediately above those for the mass distribution. This is simply due to the fact that the OPS measures the particle dimension in 16 dimension intervals, and the mass distribution is proportional to the cubic power of the particle diameter, thus favouring the higher OPS stages. An increase in the number of OPS stages would therefore bring the peaks closer together, and a real continuous measurement would lead to a complete peak overlap.

3.3. High temperature results

Fig. 8 shows the average friction coefficient curves for the compositions tested at high temperature. While no meaningful difference in this regard could be observed at room temperature (see Fig. 6), it is hereby possible to observe a different behaviour between 7Ph and the benzoxazine-bound materials in the initial part of the test: all materials show an initial COF peak, which then lowers to a steady-state value, but this initial peak is much broader in case of 7Ph (see circled area in Fig. 8). This could be explained by the lower resistance to thermal degradation of the phenolic resin binder (see Fig. 5), which makes it

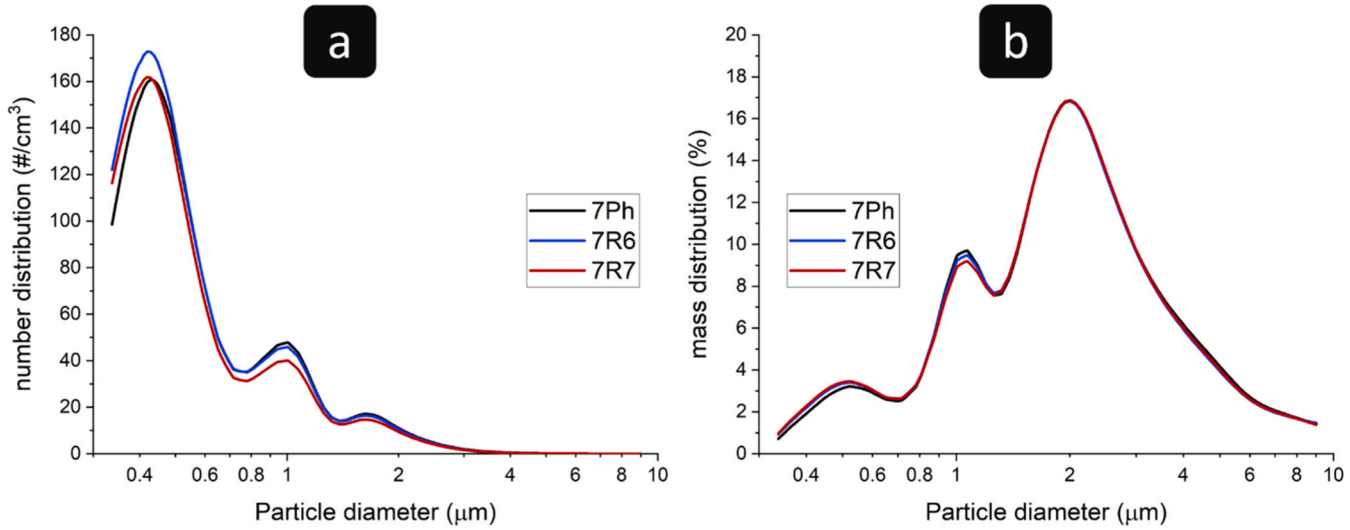

Fig. 7. Number distribution (a) and mass distribution (b) of the airborne PM produced during PoD testing.

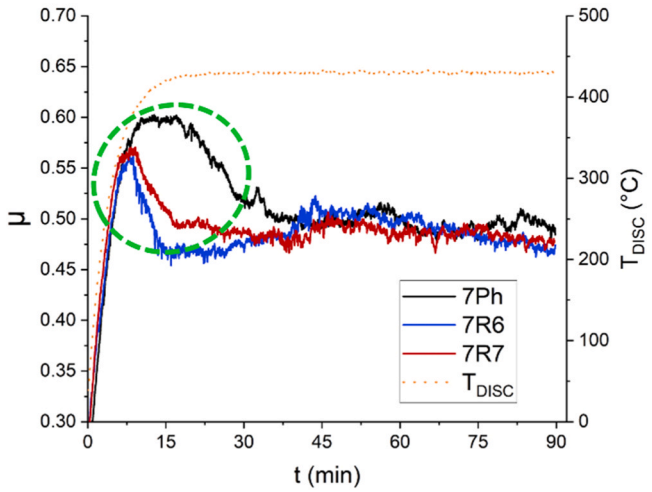

Fig. 8. Average PoD friction coefficient curves for the tested friction material compositions at the controlled high temperature of 430 °C. The orange dotted line indicated the actual temperature over the test time, while the green dashed circle highlights the COF peaks at the beginning of the tests.

more difficult for 7Ph to sustain the formation, by accumulation and compaction of wear debris, of a stable friction layer. Note that each test started from room temperature, and the actual high temperature value of 430 °C was reached slightly after the 10 min mark (see orange dotted curve in Fig. 8).

The main tribological results of the high temperature tests are collected in Table 4. Congruently with the room temperature result, the steady-state friction coefficient μ_{SS} was similar for all compositions. The volumetric wear showed more marked differences. 7R7 showed slightly lower Ka respect to 7R6, while that of 7Ph was pronouncedly higher. However, in this case the difference could not be explained by the density difference between benzoxazine- and phenolic-bound materials. Indeed, the gravimetric wear of 7Ph at high temperature was significantly higher than those of 7R6 and 7R7. The same trend could be observed regarding Ka/μ, which showed how, in harsh braking conditions, benzoxazine-bound friction materials could reach 22–32% longer operational life respect to conventionally phenolic-bound materials.

Table 4
Tribological results obtained from the PoD tests performed at the controlled high temperature of 430 °C.

Friction material	μ_{SS} (-)	Gravimetric wear (mg/km)	Ka (10^{-14} m^2/N)	Ka/μ (10^{-14} m^2/N)
7Ph	0.49 ± 0.02	5.0 ± 0.2	2.60 ± 0.11	5.14 ± 0.20
7R6	0.49 ± 0.01	4.1 ± 0.2	2.02 ± 0.07	4.21 ± 0.08
7R7	0.49 ± 0.02	3.8 ± 0.3	1.88 ± 0.11	3.90 ± 0.14

Notably, the wear values were lower than those obtained at room temperature (see Table 3), particularly in the case of 7R6 and 7R7. While seemingly counterintuitive, this result has been previously observed in metal-metal contacts [53,54]. Although this case is not exactly equivalent to that of metal-metal contact, it features some similarities, especially regarding the formation of an oxide layer in the contact region. Therefore, the higher temperature could have promoted the formation of a stronger oxidized friction layer, which counterbalanced the thermal degradation of the material, finally leading to lower overall wear. It is worth noting that this result would probably not hold true in harsher braking conditions, i.e. higher values of v_S and P_C.

Although it was not possible to investigate the PM emission at high temperature, the lower wear shown by 7R6 and 7R7 respect to 7Ph despite having extremely similar dissipated power, along with the lower thermal degradation of the benzoxazine-bound friction material (see Fig. 5), suggests that the benzoxazine-resin binder could have led to a lower production of wear debris, and thus to lower emission in harsher braking conditions. Furthermore, the lower thermal degradation of the benzoxazine-bound friction material shown in Fig. 5, might suggest a lower effect of the increase in finer PM fraction due to the overcome of the threshold temperature value for the material [3–6].

3.4. Characterization of worn surfaces

SEM analyses were carried out on the worn surfaces of the pin samples both after room temperature and high-temperature tests. No appreciable differences could be observed regarding the surface features of the different compositions, neither at room temperature nor at high temperature. However, significant changes in the friction layer developed moving from room temperature to high temperature braking conditions. Fig. 9 shows the SEM micrographs of friction layers at room and at high temperature. At RT, the primary contact plateau (steel fiber, blue outline in Fig. 9a) resulted clearly distinguishable from the secondary contact plateau (yellow outline in Fig. 9a), while at 430 °C the secondary contact plateaus ended up covering the supporting metallic

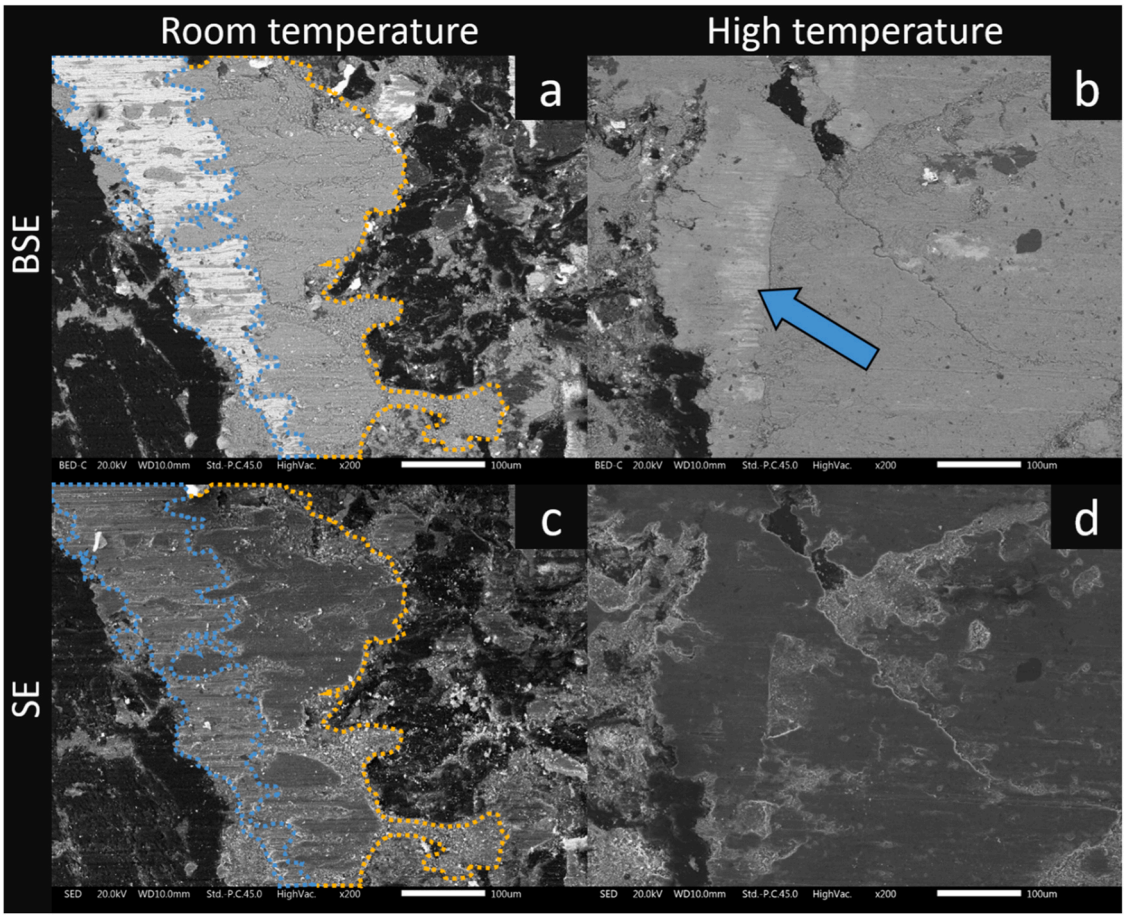

Fig. 9. Scanning electron microscope micrographs of the pin worn surface. Backscattered electron micrographs were obtained after room temperature (a) and 430 °C (b) testing. Corresponding secondary electron micrographs were obtained both after room temperature (c) and 430 °C (d) testing.

fibers, which resulted barely visible through the BSE detector. The secondary contact plateaus were much more developed after high temperature testing, as can be appreciated by comparing the extension of the grey areas in the BSE micrographs (Fig. 9a and Fig. 9b). Indeed, the steel fiber primary contact plateaus get covered by the secondary plateau particles, becoming barely visible at high temperature. Furthermore, the secondary contact plateaus also resulted much more compacted at 430 °C respect to room temperature. This is made evident by the grey-scale homogeneity showed in the high temperature SE micrograph (Fig. 9d) respect to the RT one, where some crumbling of the plateau is evident (yellow outline in Fig. 9c). These results were coherent with the friction layer theory first provided by Eriksson et al. [55,56].

The more widespread coverage of secondary contact plateaus at high temperature is a known phenomenon [57,58]. In such conditions, the accumulation and compaction of wear debris is made easier by an increase in the sintering driving force provided by the temperature [15]. Therefore, the stronger compaction of the particles in the friction layer that was hereby observed could be explained by the same mechanism: the higher temperature allowed for a more developed sintering of the wear debris. Such widespread and compact friction layers corroborate the hypothesis made in 3.2 explaining the lower wear observed in high temperature testing. However, the higher wear experienced by the phenolic-bound material at 430 °C (see Table 4) cannot be explained by the friction layer features themselves, since they appeared similar regardless of the used binder. It could therefore be explained by the failure of the friction material underneath the friction layer, which is responsible for the provision of underlying structural support to the contact plateaus. This would be caused by the lower thermal resistance of 7Ph respect to the materials bound by benzoxazine resins, as can be seen in Fig. 5.

The results of the EDXS elemental analyses carried out on the secondary contact plateaus after room and high temperature testing are shown in Table 5. Analogously to the previously mentioned topographical features of the friction layer, the compositions of the secondary contact plateaus resulted extremely similar between the different composition, showing instead marked differences between RT and 430 °C tests. For this reason, the values shown in Table 5 are an overall average of the elemental compositions of all friction material mixtures.

The concentration of Fe at high temperature was lowered respect to room temperature, however this trend was opposite for all the other elements. The high iron concentration is expected due to the strong contribution to the friction layer formation of the grey cast iron disc counterface. Furthermore, the secondary contact plateaus are well known to be constituted by mostly iron oxides. At higher temperature,

Table 5
Secondary contact plateaus EDXS results after room temperature and high temperature PoD tests.

Element	Room temperature mass (%)	High temperature mass (%)
Fe	70.9 ± 3.4	48.6 ± 2.4
O	19.5 ± 4.1	22.0 ± 4.7
Zn	2.3 ± 0.2	9.3 ± 0.5
Sn	1.5 ± 0.1	4.6 ± 0.3
Al	1.2 ± 0.2	4.3 ± 0.4
Mg	1.1 ± 0.2	3.8 ± 0.4
Others	*difference*	*difference*

the relative amount of Fe was expected to drop respect to that of oxygen due to the conditions favourable to oxidation. However, the hereby observed results also show a significant increase in presence of elements different from the conventional iron oxides. The capability of the friction layer to accommodate higher quantities of these ingredients at higher temperature might once again be explained by the stronger sintering driving force provided by the temperature.

4. Conclusions

In this study, three different friction material compositions were produced by mixing different resin binders with a commercial low-metallic friction material mixture. One composition was bound by conventional phenolic resin (Ph), while the other two were bound by two types of benzoxazine resins (R6 and R7). Room temperature and high temperature PoD testing, PM emission analysis and SEM-EDXS analysis were carried out to assess the possible benefits associated to the substitution of conventional phenolic resins with benzoxazine resins in brake pad friction materials.

- The benzoxazine-bound compositions showed lower wear, particularly at high temperature, which translates in a longer operational life of the friction material
- PM emission at room temperature was comparable between the different compositions. However, the lower high temperature wear of 7R6 and 7R7 suggests that PM emission in those conditions could be lowered by adopting a benzoxazine resin binder
- Respect to our previous study, the results hereby obtained showed how a correct processing of the friction material leads to a friction material having better tribological properties
- Despite the hereby listed advantages showcased by benzoxazine resins, the processing phase required a more energy intensive process
- The physical features and the elemental composition of the friction layer were independent of the binder used. Instead, marked differences in both physical features and elemental composition of the friction layer were observed between room temperature and high temperature tests.

Overall, benzoxazine-bound materials showed better tribological properties thanks to their lower wear. A possible environmental benefit can be envisioned through their use owing to the longer operational life bestowed to the friction material components and possibly to lower emissions in harsh braking conditions.

As for the future developments of this work, they will aim at testing these materials using a more comprehensive brake dynamometer, which would also allow for the measurement of high temperature emission. Furthermore, a LCA (Life-Cycle Assessment) analysis would be useful to better quantify any possible environmental benefit associated with the use of benzoxazine resins as brake pad friction material binder.

CRediT authorship contribution statement

Luca Fambri: Supervision, Resources, Methodology. **Davide Carlevaris:** Writing – original draft, Visualization, Methodology, Investigation, Formal analysis, Data curation, Conceptualization. **Cinzia Menapace:** Writing – review & editing, Resources, Project administration. **Giovanni Straffelini:** Writing – review & editing, Resources, Project administration.

Declaration of Competing Interest

The authors declare that they have no known competing financial interests or personal relationships that could have appeared to influence the work reported in this paper.

Data availability

Data will be made available on request.

References

[1] Dante RC. 10 - Binders and organic materials. In: Dante RC, editor. Handbook of friction materials and their applications. Boston: Woodhead Publishing; 2016. p. 135–53. https://doi.org/10.1016/B978-0-08-100619-1.00010-9.

[2] Balachandran S, Balaji S, Kathar S, Sudhan PHS. Influence of binder on thermomechanical and tribological performance in brake pad. Tribology Ind 2018; vol. 40:654–69. https://doi.org/10.24874/ti.2018.40.04.12.

[3] Joo BS, Chang YH, Seo HJ, Jang H. Effects of binder resin on tribological properties and particle emission of brake linings. Wear 2019;vol. 434–435:202995. https://doi.org/10.1016/j.wear.2019.202995.

[4] Alemani M, et al. Dry sliding of a low steel friction material against cast iron at different loads: Characterization of the friction layer and wear debris. Wear 2017; vol. 376–377:1450–9. https://doi.org/10.1016/j.wear.2017.01.040.

[5] Alemani M, Wahlström J, Olofsson U. On the influence of car brake system parameters on particulate matter emissions. Wear 2018;vol. 396–397:67–74. https://doi.org/10.1016/j.wear.2017.11.011.

[6] Alemani M, Nosko O, Metinoz I, Olofsson U. A study on emission of airborne wear particles from car brake friction pairs. SAE Int J Mater Manuf 2016;vol. 9(1): 147–57.

[7] Straffelini G, Ciudin R, Ciotti A, Gialanella S. Present knowledge and perspectives on the role of copper in brake materials and related environmental issues: a critical assessment. Environ Pollut 2015;vol. 207:211–9. https://doi.org/10.1016/j.envpol.2015.09.024.

[8] Balakrishna S, Lomnicki S, McAvey KM, Cole RB, Dellinger B, Cormier SA. Environmentally persistent free radicals amplify ultrafine particle mediated cellular oxidative stress and cytotoxicity. Part Fibre Toxicol 2009;vol. 6(1):11. https://doi.org/10.1186/1743-8977-6-11.

[9] Peikertová P, et al. Water suspended nanosized particles released from nonairborne brake wear debris. Wear 2013;vol. 306(1):89–96. https://doi.org/10.1016/j.wear.2013.07.008.

[10] Popoola LT, Adebanjo SA, Adeoye BK. Assessment of atmospheric particulate matter and heavy metals: a critical review. Int J Environ Sci Technol 2018;vol. 15 (5):935–48. https://doi.org/10.1007/s13762-017-1454-4.

[11] Samet JM, Dominici F, Curriero FC, Coursac I, Zeger SL. Fine particulate air pollution and mortality in 20 U.S. Cities, 1987–1994. N Engl J Med 2000;vol. 343 (24):1742–9. https://doi.org/10.1056/NEJM200012143432401.

[12] Pope C, et al. Lung cancer, cardiopulmonary mortality, and long-term exposure to fine particulate air pollution. JAMA: J Am Med Assoc 2002;vol. 287:1132–41. https://doi.org/10.1001/jama.287.9.1132.

[13] Kukutschová J, et al. Wear mechanism in automotive brake materials, wear debris and its potential environmental impact. Wear 2009;vol. 267(5):807–17. https://doi.org/10.1016/j.wear.2009.01.034.

[14] Xing Y-F, Xu Y-H, Shi M-H, Lian Y-X. The impact of PM2.5 on the human respiratory system *(January 2016): Journal of Thoracic Disease*, 2016, Accessed: Jan. 01 J Thorac Dis 2016;Vol 8(No 1) *(January 2016): Journal of Thoracic Disease*, 2016, Accessed: Jan. 01, ⟨https://jtd.amegroups.com/article/view/6353⟩.

[15] Straffelini G, Gialanella S. Airborne particulate matter from brake systems: an assessment of the relevant tribological formation mechanisms. Wear Aug. 2021; vol. 478–479:203883. https://doi.org/10.1016/j.wear.2021.203883.

[16] H. Dodiuk and S. Goodman, *Handbook of Thermoset Plastics*, vol. 254. 2014.

[17] Gupta MK, Hindersinn RR. Shelf life of phenolic resole resins. Polym Eng Sci 1987; vol. 27(13):976–8. https://doi.org/10.1002/pen.760271308.

[18] Jubsilp C, Rimdusit S. Chapter 44 - Polybenzoxazine-based self-lubricating and friction materials. In: Ishida H, Froimowicz P, editors. Advanced and emerging polybenzoxazine science and technology. Amsterdam: Elsevier; 2017. p. 945–74. https://doi.org/10.1016/B978-0-12-804170-3.00044-5.

[19] Holly FW, Cope AC. Condensation products of aldehydes and ketones with o-aminobenzyl alcohol and o-hydroxybenzylamine. J Am Chem Soc 1944;vol. 66 (11):1875–9. https://doi.org/10.1021/ja01239a022.

[20] Ishida H. Chapter 1 - Overview and historical background of polybenzoxazine research. In: Ishida H, Agag T, editors. Handbook of benzoxazine resins. Amsterdam: Elsevier; 2011. p. 3–81. https://doi.org/10.1016/B978-0-444-53790-4.00046-1.

[21] Wirasate S, Dhumrongvaraporn S, Allen DJ, Ishida H. Molecular origin of unusual physical and mechanical properties in novel phenolic materials based on benzoxazine chemistry. J Appl Polym Sci 1998;vol. 70(7):1299–306. https://doi.org/10.1002/(SICI)1097-4628(19981114)70:7<1299::AID-APP6>3.0.CO;2-H.

[22] Allen DJ, Ishida H. Thermosets: phenolics, novolacs, and benzoxazine. In: Buschow KHJ, Cahn RW, Flemings MC, Ilschner B, Kramer EJ, Mahajan S, Veyssière P, editors. Encyclopedia of materials: science and technology. Oxford: Elsevier; 2001. p. 9226–9. https://doi.org/10.1016/B0-08-043152-6/01662-4.

[23] Liu Y, Zhang H, Wang M, Liao C, Zhang J. Thermal degradation behavior and mechanism of polybenzoxazine based on bisphenol-S and methylamine. J Therm Anal Calorim 2013;vol. 112(3):1213–9. https://doi.org/10.1007/s10973-012-2678-7.

[24] Yang P, Wang X, Fan H, Gu Y. Effect of hydrogen bonds on the modulus of bulk polybenzoxazines in the glassy state. Phys Chem Chem Phys 2013;vol. 15(37): 15333–8. https://doi.org/10.1039/C3CP51001H.

[25] Yang P, Gu Y. A novel benzimidazole moiety-containing benzoxazine: synthesis, polymerization, and thermal properties. J Polym Sci Part A: Polym Chem 2012;vol. 50(7):1261–71. https://doi.org/10.1002/pola.25873.
[26] Yang P, Gu Y. Synthesis of a novel benzoxazine-containing benzoxazole structure and its high performance thermoset. J Appl Polym Sci 2012;vol. 124(3):2415–22. https://doi.org/10.1002/app.35305.
[27] Chirachanchai S, Phongtamrug S, Laobuthee A, Tashiro K. Chapter 4 - Mono-substituted phenol-based benzoxazines: inevitable dimerization via self-termination and its metal complexation. In: Ishida H, Agag T, editors. Handbook of benzoxazine resins. Amsterdam: Elsevier; 2011. p. 111–26. https://doi.org/10.1016/B978-0-444-53790-4.00049-7.
[28] Ishida H, NAKAMURA M. Mechanical and thermal properties of new crosslinkable telechelics with benzoxazine moiety at the chain end. Polymer 2009;vol. 50:2688–95.
[29] Endo T, Sudo A. Chapter 3 - Molecular designs of benzoxazines with enhanced reactivity based on utilization of neighboring-group participation and introduction of thioether moiety. In: Ishida H, Froimowicz P, editors. Advanced and emerging polybenzoxazine science and technology. Amsterdam: Elsevier; 2017. p. 23–33. https://doi.org/10.1016/B978-0-12-804170-3.00003-2.
[30] Bandeira C, Pereira A, Botelho E, Costa M. Benzoxazine resin and their nanostructured composites cure kinetic by DSC. J Mater Res 2013;vol. 28. https://doi.org/10.1557/jmr.2013.327.
[31] Gu Y, Li M. Chapter 3 - molecular modeling. In: Ishida H, Agag T, editors. Handbook of benzoxazine resins. Amsterdam: Elsevier; 2011. p. 103–10. https://doi.org/10.1016/B978-0-444-53790-4.00048-5.
[32] Ran Q, Gu Y, Ishida H. Chapter 11 - THermal Degradation Mechanism of polybenzoxazines. In: Ishida H, Froimowicz P, editors. Advanced and emerging polybenzoxazine science and technology. Amsterdam: Elsevier; 2017. p. 171–204. https://doi.org/10.1016/B978-0-12-804170-3.00011-1.
[33] Lu Y, Yu X, Han L, Zhang K. Recent progress of high performance thermosets based on norbornene functional benzoxazine resins. Polymers 2021;vol. 13(9). https://doi.org/10.3390/polym13091417.
[34] Zhang K, Froimowicz P, Ishida H. Chapter 4 - Development of new generation benzoxazine thermosets based on smart ortho-benzoxazine chemistry. In: Ishida H, Froimowicz P, editors. Advanced and emerging polybenzoxazine science and technology. Amsterdam: Elsevier; 2017. p. 35–64. https://doi.org/10.1016/B978-0-12-804170-3.00004-4.
[35] Verge P, Puchot L, Vancaeyzeele C, Vidal F, Habibi Y. Chapter 7 - Symmetric versus asymmetric di-bz monomer design: structure-to-properties relationship. In: Ishida H, Froimowicz P, editors. Advanced and emerging polybenzoxazine science and technology. Amsterdam: Elsevier; 2017. p. 89–107. https://doi.org/10.1016/B978-0-12-804170-3.00007-X.
[36] Menapace C, Leonardi M, Secchi M, Bonfanti A, Gialanella S, Straffelini G. Thermal behavior of a phenolic resin for brake pad manufacturing. J Therm Anal Calorim 2019;vol. 137(3):759–66. https://doi.org/10.1007/s10973-019-08004-2.
[37] Křístková M, Filip P, Weiss Z, Peter R. Influence of metals on phenol-formaldehyde resin degradation in friction composites. Polym Degrad Stab 2004;vol. 84:49–60. https://doi.org/10.1016/j.polymdegradstab.2003.09.012.
[38] Jubsilp C, Jantaramaha J, Mora P, Rimdusit S. Tribological performance and thermal stability of nanorubber-modified polybenzoxazine composites for non-asbestos friction materials. Polymers 2021;vol. 13(15). https://doi.org/10.3390/polym13152435.
[39] Gurunath PV, Bijwe J. Potential exploration of novel green resins as binders for NAO friction composites in severe operating conditions. Wear 2009;vol. 267(5):789–96. https://doi.org/10.1016/j.wear.2009.02.012.
[40] Lertwassana W, Parnklang T, Mora P, Jubsilp C, Rimdusit S. High performance aramid pulp/carbon fiber-reinforced polybenzoxazine composites as friction materials. Compos Part B: Eng 2019;vol. 177:107280. https://doi.org/10.1016/j.compositesb.2019.107280.
[41] European Commission, Proposal for a Regulation of the European Parliament and the Council on type-approval of motor vehicles and engines and of systems, components and separate technical units intended for such vehicles, with respect to their emissions and battery durability (Euro 7) and repealing Regulations (EC) *No 715/2007* and (*EC) No 595/2009* . 2022, pp. 1–66. Accessed: Feb. 07, 2023. [Online]. Available: ⟨https://eur-lex.europa.eu/legal-content/EN/TXT/?uri=CELEX:52022PC0586⟩.
[42] E. Miller and A. Arbor, Revised 2023 and Later Model Year Light-Duty Vehicle Greenhouse Gas Emissions Standards - Final rule. Environmental Protection Agency (EPA), Dec. 30, 2021. [Online]. Available: ⟨https://www.reginfo.gov/public/do/eAgendaViewRule?pubId=202204&RIN=2060-AV13⟩.
[43] Wilairat T, Saechin N, Buggakupta W, Sujaridworakun P. Effects of hot molding parameters on physical and mechanical properties of brake pads. Key Eng Mater 2019;vol. 824:59–66. https://doi.org/10.4028/www.scientific.net/KEM.824.59.
[44] Aleksendrić D, Senatore A. Optimization of manufacturing process effects on brake friction material wear. J Compos Mater 2012;vol. 46(22):2777–91. https://doi.org/10.1177/0021998311432489.
[45] Zaharudin AM, Ria Jaafar T, Berhan MN, Budin S, Aziurah M. Taguchi method for optimizing the manufacturing parameters of friction materials. Int J Mech Mater Eng 2012;vol. 7.
[46] Wang P, Liu M, Ran Q. The study on curing and weight-loss mechanisms of benzoxazine during thermal curing process. Polym Degrad Stab 2020;vol. 179:109279. https://doi.org/10.1016/j.polymdegradstab.2020.109279.
[47] Muc A, Romanowicz P, Chwał M. Description of the resin curing process—formulation and optimization. Polymers 2019;vol. 11(1). https://doi.org/10.3390/polym11010127.
[48] Carlevaris D, Menapace C, Straffelini G, Fambri L. Characterization of benzoxazine resins for brake pad friction materials manufacturing. J Therm Anal Calorim 2023;vol. 148(3):767–87. https://doi.org/10.1007/s10973-022-11789-4.
[49] Federici M, Alemani M, Menapace C, Gialanella S, Perricone G, Straffelini G. A critical comparison of dynamometer data with pin-on-disc data for the same two friction material pairs – a case study. Wear 2019;vol. 424–425:40–7. https://doi.org/10.1016/j.wear.2019.02.009.
[50] Namgung H-G, et al. Size distribution analysis of airborne wear particles released by subway brake system. Wear 2017;vol. 372–373:169–76. https://doi.org/10.1016/j.wear.2016.12.026.
[51] Wahlström J, Olander L, Olofsson U. Size, shape, and elemental composition of airborne wear particles from disc brake materials. Tribology Lett 2010;vol. 38(1):15–24. https://doi.org/10.1007/s11249-009-9564-x.
[52] Sanders PG, Xu N, Dalka TM, Maricq MM. Airborne brake wear debris: size distributions, composition, and a comparison of dynamometer and vehicle tests. Environ Sci Technol 2003;vol. 37(18):4060–9. https://doi.org/10.1021/es034145s.
[53] Stott FH. The role of oxidation in the wear of alloys. Tribology Int 1998;vol. 31(1):61–71. https://doi.org/10.1016/S0301-679X(98)00008-5.
[54] Jiang J, Stott FH, Stack MM. The role of triboparticulates in dry sliding wear. Tribology Int 1998;vol. 31(5):245–56. https://doi.org/10.1016/S0301-679X(98)00027-9.
[55] Eriksson M, Jacobson S. Tribological surfaces of organic brake pads. Tribology Int 2000;vol. 33(12):817–27. https://doi.org/10.1016/S0301-679X(00)00127-4.
[56] Eriksson M, Bergman F, Jacobson S. On the nature of tribological contact in automotive brakes. Wear 2002;vol. 252(1):26–36. https://doi.org/10.1016/S0043-1648(01)00849-3.
[57] Candeo S, Federici M, Leonardi M, Straffelini G. Brake performance maps for a Cu-free friction material with different scorching conditions. Tribology Trans 2021;vol. 64(3):540–50. https://doi.org/10.1080/10402004.2020.1869360.
[58] Öztürk B, Arslan F, Öztürk S. Effects of different kinds of fibers on mechanical and tribological properties of brake friction materials. Tribology Trans 2013;vol. 56. https://doi.org/10.1080/10402004.2013.767399.